

Green isolation of cellulosic materials from recycled pulp and paper sludge: a Box-Behnken design optimization

Evans K. Suter, Hilary L. Rutto, Tumisang S. Seodigeng, Sammy L. Kiambi & Wesley N. Omwoyo

To cite this article: Evans K. Suter, Hilary L. Rutto, Tumisang S. Seodigeng, Sammy L. Kiambi & Wesley N. Omwoyo (21 Mar 2024): Green isolation of cellulosic materials from recycled pulp and paper sludge: a Box-Behnken design optimization, Journal of Environmental Science and Health, Part A, DOI: [10.1080/10934529.2024.2331942](https://doi.org/10.1080/10934529.2024.2331942)

To link to this article: <https://doi.org/10.1080/10934529.2024.2331942>



Published online: 21 Mar 2024.



Submit your article to this journal [↗](#)



View related articles [↗](#)



View Crossmark data [↗](#)



Green isolation of cellulosic materials from recycled pulp and paper sludge: a Box-Behnken design optimization

Evans K. Suter^a , Hilary L. Rutto^a, Tumisang S. Seodigeng^a, Sammy L. Kiambi^a, and Wesley N. Omwoyo^b

^aDepartment of Chemical Engineering and Metallurgy, Clean Technology and Applied Materials Research Group, South Africa;

^bBiotechnology and Chemistry Department, Vaal University of Technology, South Africa

ABSTRACT

Cellulose was isolated from recycled pulp and paper sludge and used to synthesize cellulose nanocrystals. Response surface methodology and Box-Behnken design model were used to predict, improve, and optimize the cellulose isolation process. The optimal conditions were a reaction temperature of 87.5 °C, 180 min with 4% sodium hydroxide. SEM and TEM results revealed that the isolated cellulose had long rod-like structures of different dimensions than CNCs with short rod-like structures. The crystallinity index from XRD significantly increased from 41.33%, 63.7%, and 75.6% for Kimberly mill pulp sludge (KMRPPS), chemically purified cellulose and cellulose nanocrystals, respectively. The TGA/DTG analysis showed that the isolated cellulosic materials possessed higher thermal stability. FTIR analysis suggested that the chemical structures of cellulose and CNCs were modified by chemical treatment. The cellulose surface was highly hydrophilic compared to the CNCs based on the high water holding capacity of $65.31 \pm 0.98\%$ and $83.14 \pm 1.22\%$, respectively. The synthesized cellulosic materials portrayed excellent properties for high-end industrial applications like biomedical engineering, advanced materials, nanotechnology, sustainable packaging, personal care products, environmental remediation, additive manufacturing, etc.

ARTICLE HISTORY

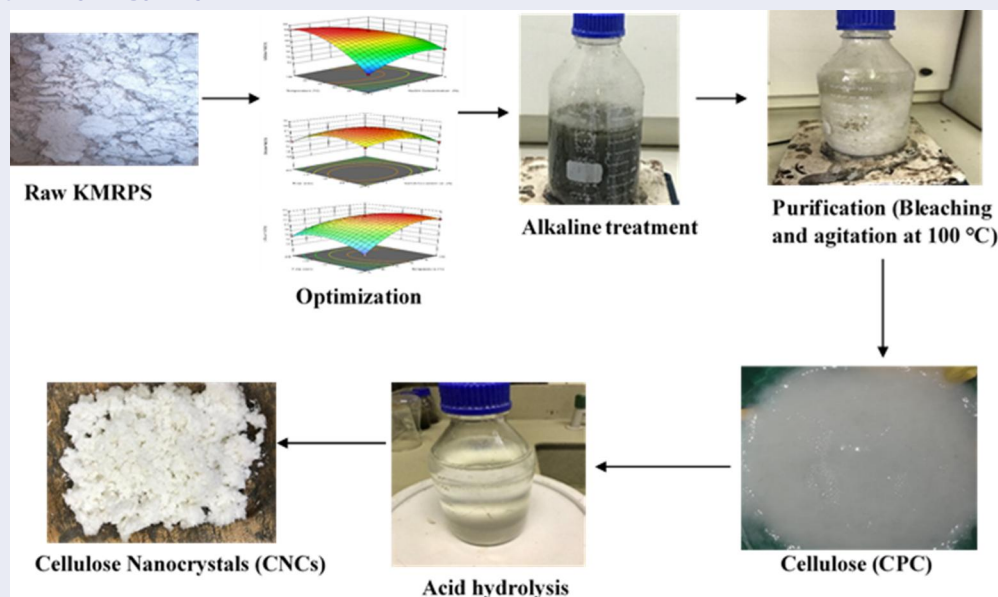
Received 7 February 2024

Accepted 5 March 2024

KEYWORDS

Box-Behnken design; recycled sludge; cellulose yield; optimization; cellulose nanocrystals

GRAPHICAL ABSTRACT



Introduction

Bio-based nanocelluloses have been the subject of in-depth study for various scientific and technological applications. They offer good values in terms of mechanical strength, aspect ratios, transparency, and chemical resistance.^[1] The pulp and paper industry stands out as an example of a technology based on a renewable resource (cellulose) in light of

the world's rapidly diminishing supply of easily exploitable material resources caused by population growth and climate change. Various processes such as viscose,^[2,3] the organosolv,^[4] the kraft,^[5] and the lyocell process,^[6] are some of the classic techniques used in the pulp and paper industries for cellulose recovery. All of these methods are efficient, but there are a few drawbacks; they pollute the environment,

have an unpleasant odor, and are unhealthy due to the solvents' toxicity. Furthermore, some products or byproducts may be challenging to use and valorize, and some organic solvents may be challenging to recycle.

One of the most significant environmental glitches is usually the enormous amount of sludge that pulp and paper mills create. Landfills are currently used for disposal, but as costs rise and land becomes more expensive, this disposal method may eventually become unaffordable.^[7] In addition, these industries must also comply with stricter environmental standards, given that the method is harmful to the environment, particularly in terms of odor and leachate.^[8]

Nanocrystalline cellulose may be produced using two different processes: (i) chemically to create cellulose nanocrystals (CNC) and (ii) mechanically to create cellulose nanofibers.^[9] These nano-cellulosic materials are perhaps attractive because of their good stiffness, high aspect ratio, low density, limited thermal expansion, simple surface modification, and low toxicity.^[10,11] These features of nanocellulose, along with its renewability and biodegradability, make it a noble, sustainable resource.^[12,13] Their rod-like shapes and relatively stable suspension provide for modest working conditions.^[14]

In this work, cellulose isolation using NaOH was based on a Box-Behnken design (BBD) model and response surface methodology (RSM) design. Sodium hypochlorite (NaOCl) was used bleaching agent in combination with sodium lauryl ether sulfate (SLES) and acetic acid. Hydrolysis was achieved using sulfuric acid (H₂SO₄) to synthesize the CNCs. Although the use of several acids for the extraction of nanocrystals from paper and pulp sludge has been described, the combination of sodium lauryl ether sulfate (SLES), sodium hypochlorite, and acetic acid under vigorous agitation in sludge cellulose fibers purification is relatively unexplored and has received very little coverage in the literature. Acid hydrolysis was used due to its rapid and simple approach to creating CNCs with improved morphological, crystallinity, and thermal characteristics. The obtained CNCs are novel for high-end applications like composites for water filtration membranes, biomedical slow-release drugs, and other industrial applications.

Materials and methods

Chemicals and reagents

Kimberly mill recycled paper sludge (KMRPPS) was used to extract the cellulose.^[15] The chemicals employed in the study were analytical grade. Sodium hydroxide (NaOH $\geq 98\%$), sulfuric acid (H₂SO₄, $> 98\%$), sodium hypochlorite (NaClO, $\geq 75\%$), sodium lauryl ether sulfate (SLES $\geq 70\%$), acetic acid ($\geq 99\%$), and acetone ($\geq 99.9\%$). The chemicals were purchased from Merck, Sigma-Aldrich, South Africa. All chemicals were used without further purification. Throughout the whole experiment, deionized water was used.

Isolation of CPC from KMRPPS

Conditioning of the sludge

The raw KMRPPS was washed twice with deionized water and retted at 50 °C for 6 h while constantly stirring to remove undesired particles. It was then air dried before being ground into small sizes and sieved through a double mesh sieve measuring 50 μm . The KMRPPS was subsequently oven-dried at 105 °C for 12 h before being stored at room temperature in sealed plastic bags.

Alkaline pretreatment

The cellulose fibers were isolated using previously reported procedures,^[16,17] with some modifications using response surface methodology (RSM) and Box-Behnken Design (BBD). The alkaline pretreatment optimization was performed under different conditions. Briefly, 100 g of KMRPPS powder was combined with 500 mL NaOH in a reactor with a concentration range of 2%–6%, temperature between (75 °C–100 °C) in a hot water bath and maintained at the same temperature with vigorous stirring at 750 rpm for 120–240 min for each experimental run. The cellulose fibers were quenched with cold water, then washed with deionized water until it was neutral in readiness for purification.

Chemical purification (bleaching)

The obtained cellulose fibers were refluxed with 350 mL (7.35% (w/v)) sodium hypochlorite, 2% (w/v) sodium lauryl ether sulfate (SLES) followed by 4 mL acetic acid. The reaction mixture was agitated for 3 h at 100 °C with constant stirring at 900 rpm. The vigorous agitation promoted the unreactive solid impurities to stick to the walls of the reactor *via* electrostatic attraction caused by the SLES added (after ionization, the anionic surfactants ionized and became negatively charged when they were applied to water and started attaching the walls of the reactor hot surface). The SLES aided in the removal of greasy stains, mud, and debris. The residue (Chemically purified cellulose) was then filtered using a Büchner funnel connected to a vacuum pump and rinsed with deionized water until it reached a neutral pH. It was then treated with acetone for 30 min in a Soxhlet chamber to remove impurities such as wax, fat, etc., and dried at room temperature for three days before acid hydrolysis.

Synthesis of CNCs through hydrolysis of CPC

In a 500 mL conical flask, 20 g of chemically purified cellulose (CPC) was combined with 400 mL (62% w/v) sulfuric acid. The synthesis process involved, using a 1:20 (g: mL) cellulose-to-acid ratio, the mixture was heated in a water bath for 45 min. The solution was first heated to 45 °C, then to 55 °C with constant stirring at 600 rpm. The hydrolysis process was stopped by carefully quenching it with 200 mL of 10-fold deionized water five times. The resultant suspension was homogenized using a centrifuge for 40 min at 4000 rpm. This process was repeated five times, each time removing the supernatant from the

Table 1. Box-Behnken design response on cellulose yield.

Run	Optimized parameters			Cellulose yield	
	A: NaOH concentration (%)	B: Temperature (°C)	C: Time (min)	Experimental yield (%)	Predicted yield (%)
1	4	87.5	180	63.97	63.98
2	4	87.5	180	63.98	63.98
3	2	100	180	64.51	64.55
4	2	87.5	120	60.97	60.96
5	4	75	120	53.75	53.82
6	6	75	180	57.45	57.41
7	4	87.5	180	64.02	63.98
8	4	100	120	62.84	62.81
9	6	87.5	120	58.36	58.33
10	2	87.5	240	58.31	58.34
11	4	100	240	56.78	56.70
12	6	87.5	240	56.69	56.70
13	4	75	240	55.65	55.68
14	2	75	180	53.78	53.71
15	4	87.5	180	63.97	63.98
16	4	87.5	180	63.97	63.98
17	6	100	180	56.51	56.58

sediment and replacing it with new distilled water until the supernatant's pH was neutral. The obtained CNCs were then allowed to dry for three days at room temperature before being characterized.

Calculation of cellulose yield

Chemical compositions of cellulose fibers obtained from KMRPPS alkali-treated were investigated at each experimental reaction point and the final optimum point. Three experimental runs of each test were performed. The modeling output and experimental data, including the cellulose yield, were calculated using Equation (1) below and presented in Table 1.

$$\% \text{ Cellulose Yield} = \left(\frac{\text{Weight of dried Cellulose}}{\text{Weight of the raw KMRPS}} \right) * 100 \quad (1)$$

Experimental design

The experimental design was performed using Response surface methodology (RSM), with a BBD modeling approach. Design-Expert 13.0.5.0 was used for surface plotting and statistical analysis. The set independent variables were (120, 180, and 240 min) reaction time, (75, 87.5, and 100 °C) reaction temperature, and NaOH concentrations of (2, 4, and 6%). In Equation (2) below, a second-order polynomial equation shows the relationship between the independent variables.

$$Y = \beta_0 + \beta_a A + \beta_b B + \beta_c C + \beta_{ab} AB + \beta_{ac} AC + \beta_{bc} BC + \beta_{aa} A^2 + \beta_{bb} B^2 + \beta_{cc} C^2 \quad (2)$$

Where A, B, and C are independent variables, Y is the anticipated results, β_0 is the model constant, β_a , β_b , and β_c are linear coefficients, β_{ab} , β_{ac} , and β_{bc} are cross-product coefficients, and β_{aa} , β_{bb} , and β_{cc} are the quadratic coefficients.

One can anticipate the reaction for certain concentrations of each component using the equation expressed in terms of coded factors. The components' high levels were set at

+1 (high level) and -1 (lower level). The coded equation compares the factor coefficients and estimates the relative significance of the components.

Characterization

The structural changes in the molecular structure of the samples were examined using Thermo Scientific Nicolet iS10 (Smart iTR) FTIR spectrometer with a diamond-based ATR compartment. The spectral resolution was set to 4 cm^{-1} over a 4000 and 500 cm^{-1} wavelength range. An average of 16 scans were captured for each spectrum, and the primary absorption peaks were identified. The thermal properties of the samples were evaluated using a thermogravimetric analysis (TGA) (Mettler Toledo) in a nitrogen atmosphere. The samples were pyrolyzed over a temperature range of $30 \text{ }^\circ\text{C}$ to $1000 \text{ }^\circ\text{C}$ at a heating rate of $10 \text{ }^\circ\text{C}/\text{min}$. The degree of crystallinity was assessed using an X-ray diffraction (Siemens D5000) diffractometer at room temperature. A monochrome step scanner Cu-K radiation set at a wavelength of 0.1538 nm , was used to scan the samples with a 2θ from 10° to 90° scan angles and 0.02 and 5.0 min scanning times. The crystallinity index (CrI) was calculated using Equation (3). Surface morphology was examined using a scanning electron microscope (JEOL-IT 7500LA, Japan) with an accelerating 15-20 kV voltage. The samples were sputtered with a thin coating of gold metal after being placed on a carbon tape metal stub. Electron diffraction spectroscopy (EDS) analysis (JSM-IT500, JEOL Ltd., Tokyo, Japan) was used to determine the CPC and CNCs percentage purity. A transmission electron microscope (TEM, Tecnai G2 20S-twin) was used to examine the morphological characteristics and particle sizes of CNCs. The samples were disseminated in a suitable solution before being put on a copper grid with a carbon layer. After drying, the samples were TEM evaluated at an accelerating voltage of 100–120 kV.

$$CrI(\%) = \frac{I_{002} - I_{am}}{I_{002}} \times 100 \quad (3)$$

Where I_{am} represents the minimum intensity ($2\theta = 15.83^\circ$) dispersed by the amorphous portion of the

Table 2. Model fit summary statistics.

Source	Std. Dev.	R ²	Adjusted R ²	Predicted R ²	Press	
Linear	0.2309	< 0.0001	0.1055	-0.1731	0.2309	
2FI	0.3360	< 0.0001	0.1585	-0.2548	0.3360	
Quadratic	< 0.0001	0.0073	0.9997	0.9982	< 0.0001	Suggested
Cubic	0.0073		1.0000			Aliased

Table 3. The sequential model sum of squares.

Source	Sum of squares	df	Mean square	F-value	p-value	
Mean vs Total	60662.39	1	60662.39			
Linear vs Mean	68.22	3	22.74	1.63	0.2309	
2FI vs Linear	50.13	3	16.71	1.27	0.3360	
Quadratic vs 2FI	131.29	3	43.76	10260.94	< 0.0001	Suggested
Cubic vs Quadratic	0.0280	3	0.0093	19.84	0.0073	Aliased
Residual	0.0019	4	0.0005			
Total	60912.06	17	3583.06			

Table 4. ANOVA for RSM quadratic model.

Source	Sum of squares	df	Mean square	F-value	p-value	
Model	0.0299	7	0.0043			Significant
Residual	0.0280	3	0.0093	19.84	0.0073	
Lack of fit	0.0019	4	0.0005			Significant
Pure Error	249.67	16				
Cor Total	0.0299	7	0.0043			

sample and I_{002} denotes the maximum intensity ($2\theta = 22.75^\circ$) of the 002 lattice diffraction peak.^[18]

Results and discussions

RSM model selection and regression analysis

A regression model was created using Design-expert 13.0.5.0. Equation (4) was used to evaluate the experimental data and it represents the cellulose yield as a function of the independent variables (time, temperature, and NaOH concentration). The summary sequential statistics, sum of squares, variance analysis for the quadratic model, and the p -value from the RSM model are provided in Tables 2–6. From the model employed, the sum of squares analysis indicated that only the quadratic model had a p -value of 0.0001 (Table 2), indicating its significance. The variance analysis demonstrated that the quadratic model was suitable for the experimental design, evidenced by its F-value of 6503.60 and lack of fit mean square value of 0.0043 (Table 4). The coefficient of determination, R^2 , measures how well the model fits the data and represents the ratio of explained variation to total variation. A high R^2 score suggests the importance of the model's dependent variables. The quadratic model's R^2 value in this study was 0.9982 (Table 3), indicating its ability to successfully explain the system's behavior. The Model F-value of 6503.60 provided more evidence for the significance of the model. Such a large F-value would occur due to noise only 0.01% of the time. Since the observed p -values for several important model terms, including A, B, C, AB, AC, BC, A², B², and C², were less than 0.0500, these terms were considered significant (Table 6). Model terms are considered irrelevant if they have values greater than 0.1000. The model reduction can improve the overall model if there are multiple unnecessary terms (apart from those required

to maintain hierarchy). The lack of fit F-value of 19.08 indicated the seriousness of the lack of fit. There was a 0.73% chance that noise is the root cause of a high lack of Fit F-value. With a difference of less than 0.2, the expected R^2 of 0.9982 and the corrected R^2 of 0.9997 were relatively consistent. The optimal value for Adeq Precision, which gauges the signal-to-noise ratio, is at least 4. In this instance, a strong signal is indicated by the ratio of 216.369. The lack of fit study confirmed the model's suitability and revealed the significance of several important model elements. With a strong signal-to-noise ratio, the model was confidently used to explore the design space.

Equation (4) below is the resulting equation expressed in terms of coded factors;

$$= 63.98 - 1.07A + 2.50B - 1.06C - 2.92AB + 0.2475AC - 1.99BC - 2.30A^2 - 3.62B^2 - 3.10C^2 \quad (4)$$

Where Y, A, B, and C are the coded variables for cellulose yield concentration, sodium hydroxide concentration, reaction temperature, and reaction time, respectively.

The variance inflation factor (VIF) is a diagnostic measure used to assess the severity of multi-collinearity, which occurs when there is a high correlation among the factors in the model. In an orthogonal design where the factors are uncorrelated, the VIFs for all factors are equal to 1 since there is no multi-collinearity. However, when the variables are correlated, there are several VIFs, and the greater the VIF, the stronger the factors are associated. VIF values less than 10 are typically regarded as acceptable, suggesting that the amount of multi-collinearity is not too severe. From the model, all the VIF values were less than 10 suggesting that the level of multi-collinearity was not problematic (Table 5).

Table 5. Coefficients in terms of coded factors.

Factor	Coefficient estimate	df	Standard Error	95% CI Low	95% CI high	VIF
Intercept	63.98	1	0.0292	63.91	64.05	
A-Concentration	-1.07	1	0.0231	-1.12	-1.02	1.0000
B-Temperature	2.50	1	0.0231	2.45	2.56	1.0000
C-Time	-1.06	1	0.0231	-1.12	-1.01	1.0000
AB	-2.92	1	0.0327	-2.99	-2.84	1.0000
AC	0.2475	1	0.0327	0.1703	0.3247	1.0000
BC	-1.99	1	0.0327	-2.07	-1.91	1.0000
A ²	-2.30	1	0.0318	-2.37	-2.22	1.01
B ²	-3.62	1	0.0318	-3.70	-3.55	1.01
C ²	-3.10	1	0.0318	-3.18	-3.03	1.01

Table 6. p-Value shading: $p < 0.05$ $0.05 \leq p < 0.1$ $p \geq 0.1$.

	Intercept	A	B	C	AB	AC	BC	A ²	B ²	C ²
Yield (1)	63.982	-1.07	2.50125	-1.06125	-2.9175	0.2475	-1.99	-2.296	-3.6235	-3.1035
p-Values		< 0.0001	< 0.0001	< 0.0001	< 0.0001	< 0.0001	< 0.0001	< 0.0001	< 0.0001	< 0.0001

Effect RMS variables interaction and optimization

Response surface plots are graphical representations that visualize the relationship between two independent variables (factors) and the response variable of interest while holding other variables at a fixed level, typically zero. These plots allow us to understand the interaction effects between the factors on the response. Elliptical response surface plots indicate a substantial interaction between the variables. The elliptical shape suggests that the interaction between the factors is significant and that their combined effects have a notable impact on the response variable. The elongated and distorted shape of the plot signifies a strong interaction effect. On the other hand, circular contour plots indicate a minor interaction between the variables. The circular shape suggests that the interaction between the factors is not substantial, and their combined effects have a relatively minimal impact on the response variable. The contours are more symmetric and less distorted, indicating a weaker interaction effect.^[16]

The results showed that there is a high agreement between the experimental data and the predicted data along the $Y = X$ line. A 2% error exists between the observed and anticipated values, according to the residual distribution map for 17 experimental runs in Figure 1. The little difference between experimental and anticipated data demonstrates a strong link. The model’s unbiased nature, demonstrated by the randomly distributed residuals along the zero line, demonstrates that all of the model’s significant elements were taken into account.

The effect of temperature and sodium hydroxide concentration on cellulose yield is shown in Figure 2. Among these parameters, sodium hydroxide concentration stands out as a significant factor influencing the disintegration of non-cellulose components and the increase in cellulose yield. The graph reveals that lower concentrations of sodium hydroxide do not contribute to a significant increase in cellulose yield. However, as the concentration surpasses a certain threshold, the cellulose yield starts to rise. This shows that for efficient cellulose extraction from the raw material, a sufficient level of sodium hydroxide must be present. Within the optimal range, reaction temperatures between 87.5 °C and 100 °C and sodium hydroxide concentrations between 2.6% and

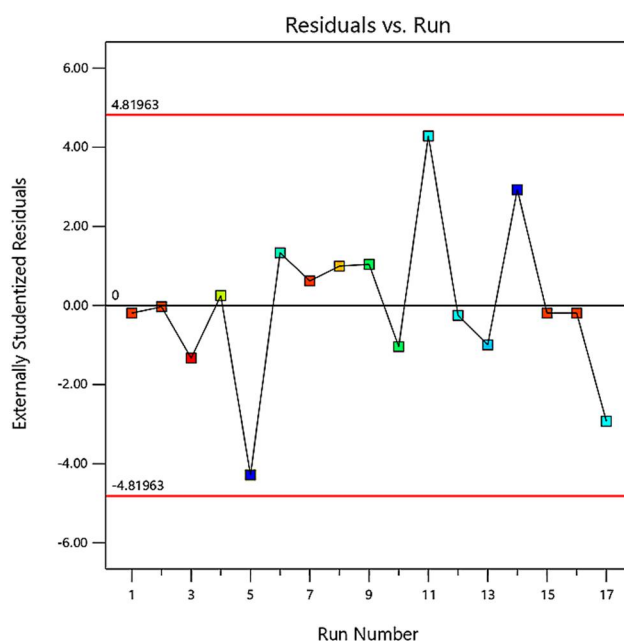


Figure 1. Residual distribution map.

5.5% resulted in the highest cellulose yield. These parameters balance extraction effectiveness with cellulose deterioration.

Consequently, the breakdown of cellulose into individual sugar molecules takes place when the sodium hydroxide concentration surpasses this range and the reaction temperature increases further. The increased temperature and excessive sodium hydroxide content contributed to the overreaction. A high sodium hydroxide concentration causes the reaction mixture to produce an excess of hydroxide ions (OH⁻), enhancing the hydrolysis reaction and speeding up the breakdown of cellulose. The kinetic energy of the reactant molecules is increased by greater temperatures, which causes more frequent and energetic collisions that accelerate the destruction of cellulose.

Figure 3 illustrates how reaction time and sodium hydroxide concentration influenced cellulose isolation. The graph shows that reaction time is a critical factor in the disintegration of non-cellulose materials during the alkali treatment process. Because the fiber’s reaction cannot be fully

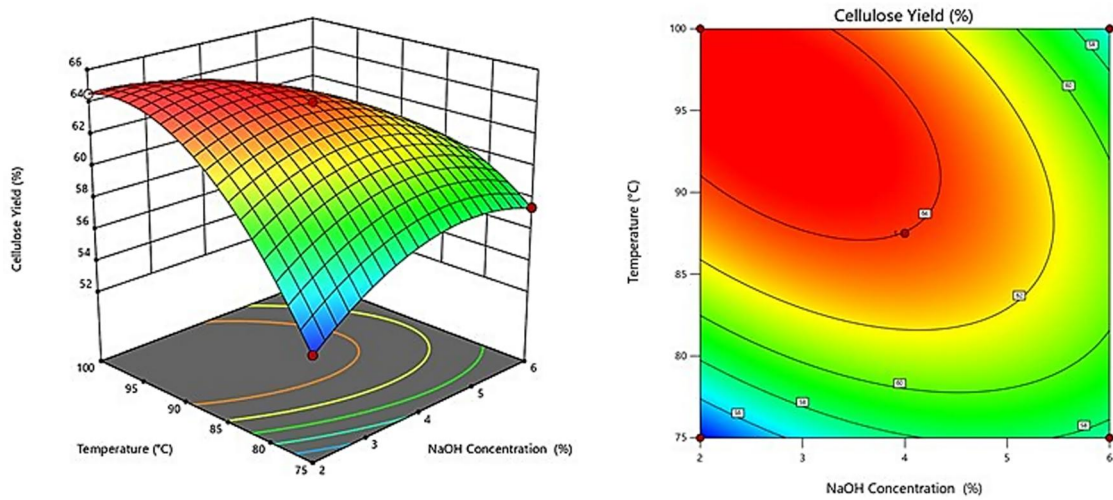


Figure 2. Impact of temperature and sodium hydroxide concentration on cellulose yield.

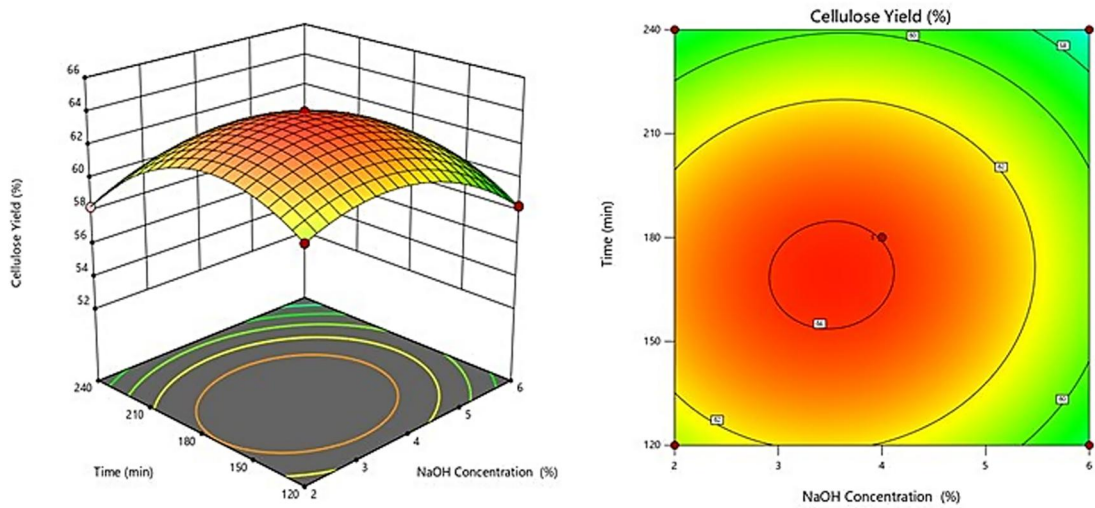


Figure 3. Effects of sodium hydroxide concentration and reaction time on cellulose yield.

triggered in a short period, a limited amount of cellulose was initially produced. However, as soon as the response time reached a specific threshold, the cellulose yield began to increase. The excellent cellulose yield is achieved within a certain range of sodium hydroxide concentration and reaction time. In this instance, the maximum yield was achieved when the reaction time was between 135 and 190 min and the sodium hydroxide concentration was between 2.5% and 5%. These conditions allowed for the efficient breakdown of non-cellulose components and cellulose extraction from the raw material. On the other hand, with longer response times, cellulose yield falls, mostly because of overreaction. Cellulose degrades excessively when the reaction is too protracted and the fiber is exposed to the alkali solution for a lengthy period. This causes cellulose to disintegrate into its component sugar molecules, lowering the yield of cellulose in the process.^[19]

Figure 4 illustrates how reaction temperature and time affect cellulose isolation. The graph emphasizes the critical part that reaction time plays in cellulose production and

KMRPPS degradation. At first, the fiber's alkali treatment might not be finished promptly, which would result in a low cellulose yield. However, the yield of cellulose starts to rise when the reaction time lengthens to a certain extent. The best conditions for cellulose synthesis are seen within a particular range of reaction temperature and time. The maximum yield may be obtained when the reaction temperature is between 87.5 °C and 100 °C and the reaction time is between 150 and 190 min. An ideal cellulose yield is obtained within this range because the KMRPPS is successfully broken down. The cellulose yield, however, drops owing to overreaction when the response time exceeds the ideal range. Excessive reaction time causes the fiber to be exposed to the alkali solution for an extended period, which causes cellulose to disintegrate into its constituent parts. Less cellulose is produced as a result of this breakdown.

According to the response surface methodology (RSM), the optimal conditions for cellulose isolation are a reaction temperature of 87.5 °C, a reaction time of 180 min, and a sodium hydroxide concentration of 4%. Under these

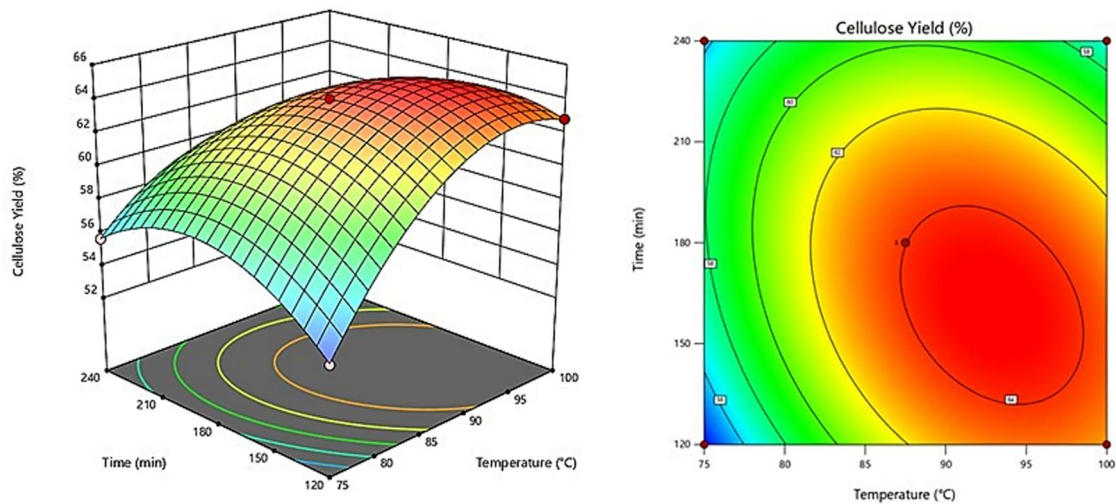


Figure 4. Effect of reaction temperature and time on cellulose yield.

conditions, the cellulose yield from KMRPPS fiber is predicted to reach 63.98%, which is not significantly different from the estimated value of 64.05% at a 95% confidence interval.

Water holding capacity (WHC)

The ability of the material to absorb water is an important consideration when creating composite materials since it significantly impacts the dimensional stability, porosity, tensile strength, and swelling behavior of natural composite materials.^[20] The physical and chemical characteristics of the fiber material and fiber processing have a significant impact on WHC.^[21] The synthesized CNCs presented a lower WHC than the isolated cellulose, with values of $65.31 \pm 0.98\%$ and $83.14 \pm 1.22\%$, respectively. The higher WHC of CPC in contrast to KMRPPS ($53.07 \pm 1.23\%$) and CNCs is due to the arrangement of fibrils, which allows water molecules to penetrate the core matrix.^[22] However, the drop in size from micrometers (μm) to nanometers (nm) generated smaller nanocrystals that are more uniform in size and have a specific surface area, contributing to CNCs' ability to allow water permeation resulting in low WHC. According to Razali et al. (2015), CNCs reduce water penetration by lowering the free volume in the fiber intermolecular chain.^[23]

Membrane filtration systems are highly desired for their ability to restrict water absorption and avoid swelling for a variety of reasons. The membrane may enlarge as a result of excessive water absorption, jeopardizing its structural integrity and creating several problems. Swollen membranes are more likely to become clogged with biomolecules or particulate debris, which lowers separation effectiveness and increases fouling. Furthermore, membranes with poor water-holding capacity have better concentration polarization resistance. Concentration polarization happens during filtration when solutes gather close to the membrane surface, reducing flow and decreasing separation effectiveness. The degree of concentration polarization can be minimized, improving membrane performance and boosting throughput

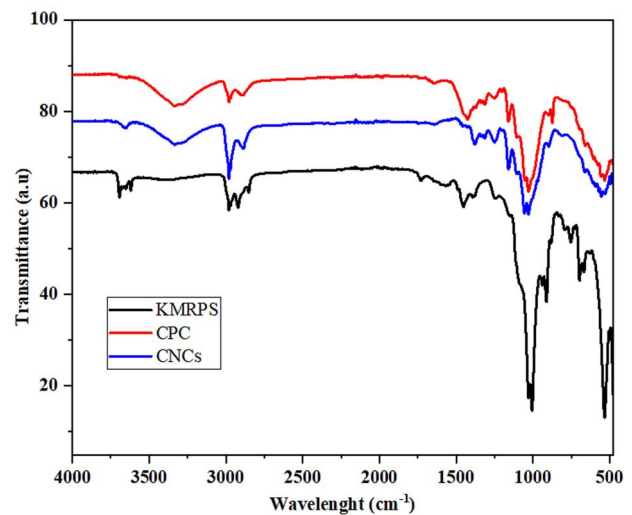


Figure 5. FTIR spectra of the raw sludge, CPC and CNCs.

by limiting water absorption. As it helps to maintain a greater and more reliable filtering rate while retaining the appropriate separation efficiency.

Spectroscopic properties

Figure 5 shows the FTIR spectra of the samples, it is clear that there are no hydroxyl functional groups present in the Kimberly mill pulp sludge (KMRPPS). This indicated that other inorganic and organic compounds in the sludge could have occupied all the OH- groups. However, after alkaline pretreatment and chemical purification, a noticeable change occurred. The OH⁻ stretching band near 3323 cm^{-1} appeared for CPC and cellulose nanocrystals (CNCs), suggesting that the alkaline pretreatment exposed the hydroxyl groups. In KMRPPS, a triplet peak between 2979 and 2878 cm^{-1} corresponds to the C-H stretching of aldehydes and ketones.^[24] Upon alkaline treatment, this triplet peak transforms into a doublet with a slight shift in the wavelength band position to 2867 and 2937 cm^{-1} . The observed bands are attributed to aliphatic symmetric and asymmetric C-H stretching.

Similarly, the peak at 1734 cm^{-1} , associated with the C=O stretching of aliphatic-aromatic ketones and hemicellulose, disappears after subsequent alkaline pretreatment and bleaching of the sludge.^[25] Furthermore, the 1455 and 1448 cm^{-1} peaks in KMRPPS and CPC are linked to C-O-H in-plane bending for carboxylic acids. These peaks vanish through acid hydrolysis to obtain CNCs. The band observed at $1330\text{--}1380\text{ cm}^{-1}$ corresponds to the bending vibrations of the C-H and C-O groups of the polysaccharides present in the sludge and the CPC. After acid hydrolysis, this peak is eliminated. Consequently, the symmetric bending of CH_2 at 1428 cm^{-1} in CNCs is associated with cellulose I. The peaks at 1245 and 1252 cm^{-1} in the sludge and CPC are attributed to the presence of hemicellulose. The reduction of this peak in the CNCs suggested its successful synthesis. Furthermore, aromatic ethers exhibit a strong band near 1250 cm^{-1} . The absorbance peaks in the 1167 and 1163 cm^{-1} range are assigned to C-O-C asymmetric stretching vibrations associated with cellulose I and cellulose II in the sludge and CPC. Peaks at 1020 , 1040 , and 1038 cm^{-1} are the polymers' main characteristic cellulose peaks. In KMRPPS, the peak at 915 cm^{-1} is attributed to α -D glucose and β -D glucose.^[24] Peaks at 879 , 898 , and 882 cm^{-1} are associated with S-O stretching in sulfonate compounds. Stretching vibrations assigned to the C-S linkage occurs in the region of $700\text{--}600\text{ cm}^{-1}$, as compounds containing C-S and S-S bonds, such as sulfides and mercaptans, exhibit stretching bands in

this region. Brominated compounds appear in the infrared spectrum's $600\text{--}500\text{ cm}^{-1}$ region.^[26,27] Most of these peaks are seen to diminish or reduce in intensity after the subsequent isolation and hydrolysis, respectively.

Morphological properties

The SEM images of raw KMRPPS, CPC, and CNCs are shown in Figure 6(a-c), together with the TEM image of CNCs (Figure 6d). The raw materials display regular rod-like structures that are not chemically connected with spongy-like materials stuck on their surface indicating that the materials are of different composition. When subjected to alkaline pretreatment and purification, the CPC portrayed rod-like structures of different dimensions with a coiled and flat shape and a smooth surface (Figure 6b). On acid hydrolysis and ultrasonication of CPC the fibers disintegrated into short rod-like structures (CNCs) as seen in the SEM micrograph (Figure 6c) and the TEM picture in Figure 6(d).^[28] The nanocrystals are reported to create a network structure that resembles a web, increasing the composite material's reinforcing capacity. From the calculated particle size distributions of CNCs using ImageJ- ij153 software, the bulk of the nanocrystals present in the dispersion had dimensions between 48 and 64 nm in width and 126 to 392 nm in length (Figure 6d). Meanwhile, strong H-bonding between the cellulose nanocrystals resulted in the

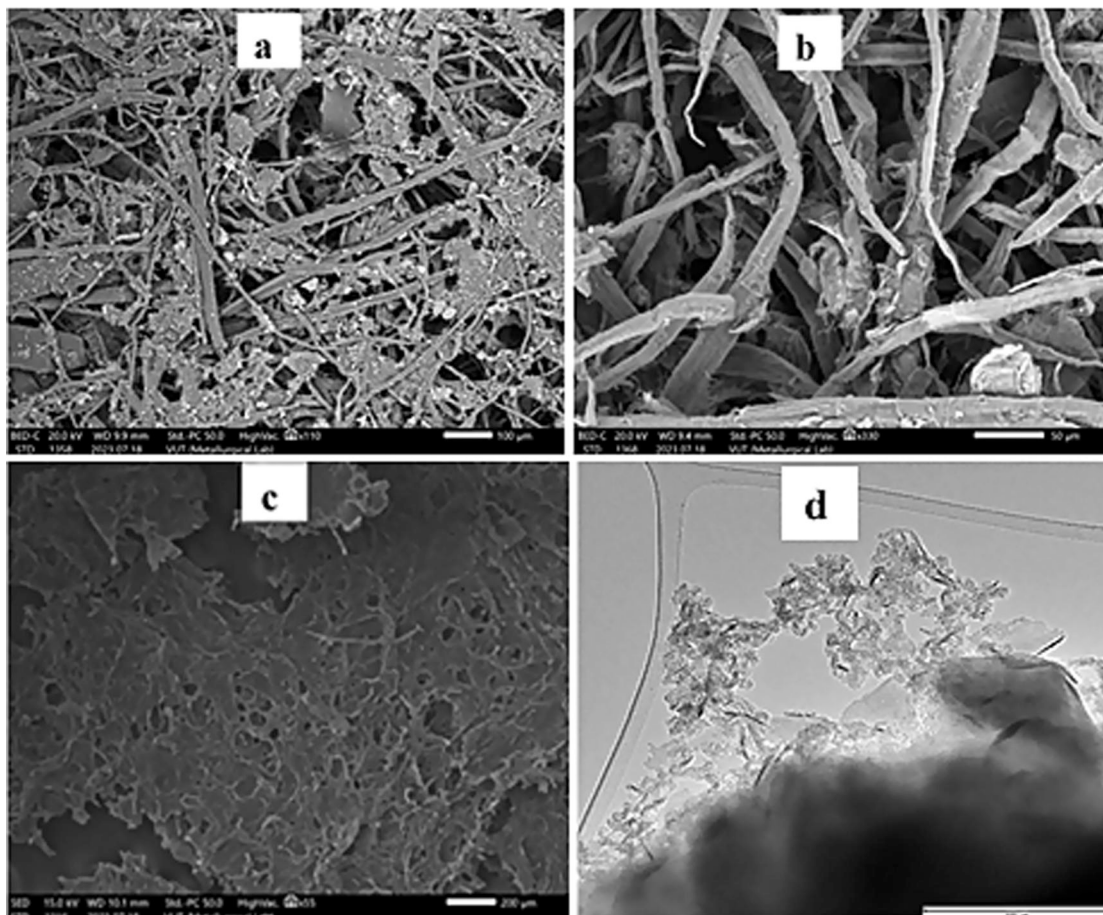


Figure 6. SEM images of raw KMRPPS, CPC, and CNCs (a-c), and TEM image of CNCs (d).

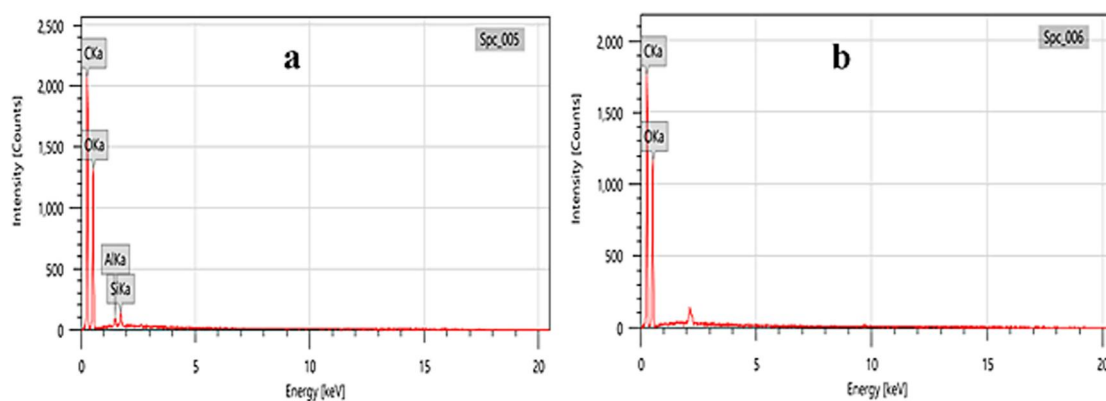


Figure 7. EDS spectrum of CPC (a), and CNCs (b).

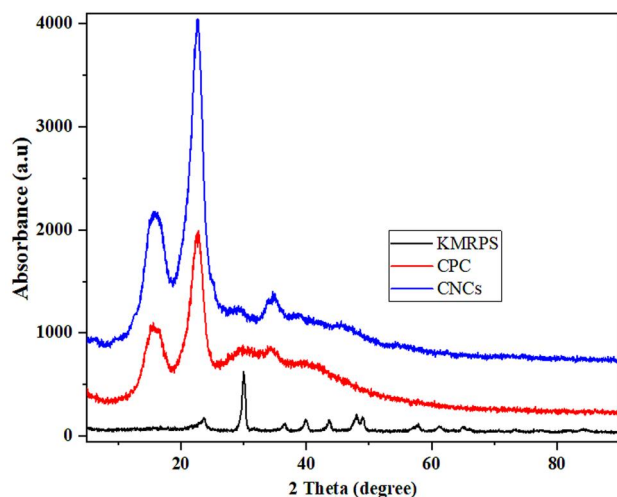


Figure 8. XRD patterns of KMRPPS, CPC and CNCs.

development of self-assembled networks, which can be attributed to the reduced degree of agglomeration of the nanocrystals.^[29]

Elemental composition

The electron dispersive spectroscopy (EDS) analysis was further investigated to confirm the composition of the isolated cellulose from the KMRPPS and the synthesized CNCs (Figure 7a,b). From the EDS spectrum, it was noted that the isolated cellulose was composed of C and O, the main building blocks of cellulose with small impurities of Al and Si from kaolinite, which is the main ingredient in pulp and paper industries. This is still noticeable in the SEM image (Figure 6b), that the cellulose fibers were not completely purified. On acid hydrolysis to produce CNCs, the impurities were eliminated leaving C and O as the main constituents of the nanocrystalline cellulose. This confirmed that the isolation of cellulose and synthesis of its nanocrystals was successfully achieved.

Crystal properties

The XRD patterns of the KMRPPS and cellulosic materials are shown in Figure 8. Three diffraction peaks, which

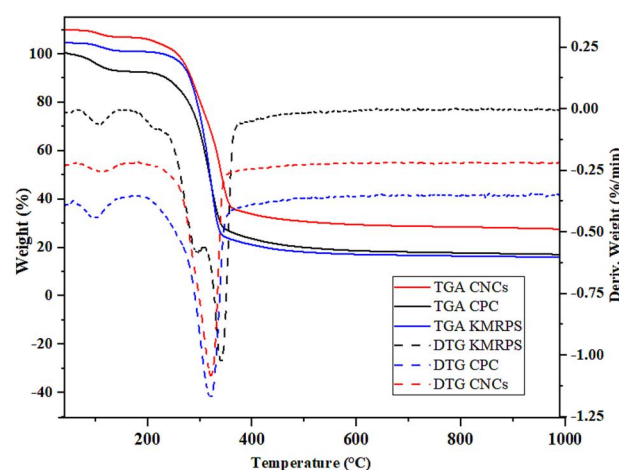


Figure 9. TGA curves (complete curves), and DTG curves (dotted curves) of KMRPPS, CPC, and CNCs.

correspond to the (110), (200), and (004) crystallographic planes of the monoclinic cellulose $I\beta$ lattice, can be seen in the cellulosic samples at $2\theta = 15.83^\circ$, 22.75° , and 34.63° , respectively.^[30] In contrast to the raw sludge, which showed a large number of peaks at various 2θ values, corresponding to calcite (CaCO_3), with the peaks at 17.10° , 23.86° , 30.14° , and 36.57° matching (JCPDS 47-1743),^[31] the diffraction peak at 39.79° was connected to crystalline carbon.^[32] The high diffraction peak at 43.82° with the JCPDS number (JCPDS card No. 5-0490) was linked to the quartz phase, such as SiO_2 .^[31,33] Further kaolinite ($\text{AlSiO}(\text{OH})$) peak at 50.07° , which was validated by JCPDS (JCPDS card No. 06-0221), corresponded with the elemental analysis that found Al and Si to be present in the sludge.^[32] This implied that the isolation and synthesis of cellulosic materials from the KMRPPS were achieved. The percentage crystallinity indices (*CrI*) of the raw sludge, CPC, and CNCs were found to be 41.33%, 63.7%, and 75.6%, respectively. This suggested that the CPC and CNCs' crystalline structure was still being formed during the nanocrystallization process. The breakdown of amorphous and disordered cellulose areas can be used to explain the increase in the crystallinity index for CNCs. Figure 8(a) demonstrates how the 22.7° and 35.4° peaks become sharper, suggesting greater crystal lattice perfection in CNCs than CPC in the (200) and (004) planes.

Increased tensile strength and thermal stability are connected with increased crystallinity index in CNCs, which is believed to be advantageous for creating high-strength composite materials.^[34] In previous studies, subsequent chemical treatments enhanced the cellulose's crystallinity.^[17] The crystallinity of cellulose has a significant role in determining its thermal stability, elasticity, and other physical properties that are crucial for various industrial applications. An increase in crystallinity makes a substance more rigid and stiff, which boosts its strength. As a result, it becomes possible to create nanocomposites with improved mechanical characteristics.^[35] When compared to prior research, the approach adopted here for the fabrication of CNCs produced somewhat greater levels of crystallinity.

Thermal properties

Figure 9 displays the TGA and DTG curves of the KMRPPS, CPC, and CNCs. All the materials experienced two weight loss stages at different temperatures except the KMRPPS which experienced three degradation stages. For the three samples, the first weight loss began at around 46 °C and continued until a maximum temperature (T_{max}) of 137 °C. This deterioration was related to the samples' loss of moisture content. According to the graphs, CPC had the greatest moisture level of roughly 8%, whereas KMRPPS and CNCs had about 6% and 4% moisture content, respectively. The second degradation process for KMRPPS began at roughly 164 °C, which is linked to the sludge's organic matter degradation temperature.^[36] The second KMRPPS degradation process began at about 200 °C, which is the beginning temperature for lignin breakdown.

The lignin component of biomass decomposes relatively slowly across a wider temperature range (200–800 °C) than the cellulose and hemicellulose components.^[37] Previous research has shown that DTG curves of lignin breakdown have flat peaks with a sloping baseline, making it hard to quantify activation energy for the reaction since there is a flat tailing section at higher temperatures.^[38] This is not the case for the sharper and more obvious DTG peaks of cellulose and hemicellulose which explained the absence of the lignin degradation peak.^[37]

The breakdown of hemicelluloses is ascribed to the degradation of KMRPPS observed between (287 to 368 °C) with a T_{max} of about 285 °C.^[23] The cellulose degradation is responsible for the degradation peak visible in the KMRPPS curve at a T_{max} of roughly 335 °C. The CPC degraded between 230 °C and 351 °C, with a T_{max} around 314 °C, whereas the CNCs declined between 237 °C and 356 °C, with a T_{max} around 316 °C.

Generally, depolymerization, dehydration, and glycosyl unit breakdown occur during cellulose's heat degradation. According to all of the aforementioned findings, CNCs have more thermal stability than cellulose raw materials, which in turn have greater thermal stability than sludge. This can be explained by the fact that crystalline order, which rises following nanocrystallization, affects the heat stability of cellulose.^[39] Additionally, the presence of surface sulfated groups

during sulfuric acid hydrolysis can dramatically reduce the breakdown temperature.^[12] The strong thermal characteristics of CNCs may expand the uses for cellulose fibers, particularly at processing temperatures beyond 200 °C for biocomposites.

Conclusion

The research established that cellulose can be isolated from recycled pulp and paper sludge. The removal of non-cellulosic materials can be improved by optimizing the process and using NaOH during alkaline pretreatment with purification aided by sodium lauryl ether sulfate (SLES). The crystallinity of the obtained nanocrystals increased, indicating that the crystalline phase was exposed after the hemicelluloses with the small portions of lignin and other organic and inorganic components were successfully eliminated. The particle size was considerably decreased in diameter after acid hydrolysis of cellulose, as revealed by TEM, indicating better CNC characteristics. The findings indicate that paper sludge, which is a threat to all pulp and paper sectors, may be used successfully exploited and used for various advantageous purposes since they are sustainable and biodegradable. Investigations into the suitability of the cellulosic materials and respective composite materials, on environmental remediation will provide valuable insights into their potential industrial and commercial applications, driving further innovation in these fields.

Acknowledgments

The authors are thankful to Kimberly Clark Paper Mill for providing the paper sludge. The Vaal University of Technology for offering laboratory space, FTIR, and SEM-EDS analysis. The North West University for the TGA and TEM analysis and The University of Witwatersrand for XRD analysis.

Authors' contributions

Mr. Evans Suter wrote the manuscript, collected the samples, and set up the experiments. Prof. Hilary Rutto provided the chemicals, coordinated sample characterization, and proofread the draft article. Prof. S.L. Kiambi was involved in the article development, data analysis, and proofreading. Prof. T.S. Seodigeng assisted in the characterization and proofreading of the draft manuscript. Dr. W.N. Omwoyo contributed to the analysis and proofreading of the manuscript.

Disclosure statement

All the authors declare no competing interests.

Funding

The authors have received no funding support from any institutions or organizations.

ORCID

Evans K. Suter  <http://orcid.org/0000-0003-1316-6889>

Data availability statement

This article includes all of the data generated or analyzed during this research.

References

- [1] Future Markets, Inc. The Global Market for Cellulose Nanofibers to 2030. **2018** (accessed Aug. 2023). <https://www.marketresearch.com/Future-Markets-Inc-v3760/Global-Cellulose-Nanofibers-12045523/>.
- [2] Li, H.; Legere, S.; He, Z.; Zhang, H.; Li, J.; Yang, B.; Zhang, S.; Zhang, L.; Zheng, L.; Ni, Y. Methods to Increase the Reactivity of Dissolving Pulp in the Viscose Rayon Production Process: A Review. *Cellulose* **2018**, *25*, 3733–3753. DOI: [10.1007/s10570-018-1840-1](https://doi.org/10.1007/s10570-018-1840-1).
- [3] Wilkes, A. G. The Viscose Process. *Regen. Cellul. Fibre*. **2001**, 37–61. ISBN 1 85573 459 1
- [4] Brosse, N.; Hussin, M. H.; Rahim, A. A. Organosolv Processes. *Biorefineries* **2019**, 153–176. DOI: [10.1007/10_2016_61](https://doi.org/10.1007/10_2016_61).
- [5] Lahtinen, M. H.; Mikkilä, J.; Mikkonen, K. S.; Kilpeläinen, I. Kraft Process—Formation of Secoisolaricresinol Structures and Incorporation of Fatty Acids in Kraft Lignin. *J. Agric. Food Chem.* **2021**, *69*, 5955–5965. DOI: [10.1021/acs.jafc.1c00705](https://doi.org/10.1021/acs.jafc.1c00705).
- [6] Elsayed, S.; Viard, B.; Guizani, C.; Hellsten, S.; Witos, J.; Sixta, H. Limitations of Cellulose Dissolution and Fiber Spinning in the Lyocell Process Using [mTBDH][OAc] and [DBNH][OAc] Solvents. *Ind. Eng. Chem. Res.* **2020**, *59*, 20211–20220. DOI: [10.1021/acs.iecr.0c04283](https://doi.org/10.1021/acs.iecr.0c04283).
- [7] Haile, A.; Gelebo, G. G.; Tesfaye, T.; Mengie, W.; Mebrate, M. A.; Abuhay, A.; Limeneh, D. Y. Pulp and Paper Mill Wastes: Utilizations and Prospects for High Value-Added Biomaterials. *Bioresour. Bioprocess.* **2021**, *8*, 1–22. DOI: [10.1186/s40643-021-00385-3](https://doi.org/10.1186/s40643-021-00385-3).
- [8] Gupta, G. K.; Liu, H.; Shukla, P.; Mandeep. Pulp and Paper Industry-Based Pollutants, Their Health Hazards and Environmental Risks. *Curr. Opin. Environ. Sci. Health* **2019**, *12*, 48–56. DOI: [10.1016/j.coesh.2019.09.010](https://doi.org/10.1016/j.coesh.2019.09.010).
- [9] Kurniawan, T. W.; Sulistyarti, H.; Rumhayati, B.; Sabarudin, A. Cellulose Nanocrystals (CNCs) and Cellulose Nanofibers (CNFs) as Adsorbents of Heavy Metal Ions. *J. Chem.* **2023**, *2023*, 1–36. DOI: [10.1155/2023/5037027](https://doi.org/10.1155/2023/5037027).
- [10] Hao, W.; Wang, M.; Zhou, F.; Luo, H.; Xie, X.; Luo, F.; Cha, R. A Review on Nanocellulose as a Lightweight Filler of Polyolefin Composites. *Carbohydr. Polym.* **2020**, *243*, 116466. DOI: [10.1016/j.carbpol.2020.116466](https://doi.org/10.1016/j.carbpol.2020.116466).
- [11] Tlou, S.; Suter, E.; Alfred, M.; Rutto, H.; Omwoyo, W. In Situ Capping of Silver Nanoparticles with Cellulosic Matrices from Wheat Straws in Enhancing Their Antimicrobial Activity: Synthesis and Characterization. *J. Environ. Sci. Health. A Tox. Hazard. Subst. Environ. Eng.* **2023**, *58*, 903–913. DOI: [10.1080/10934529.2023.2260295](https://doi.org/10.1080/10934529.2023.2260295).
- [12] Rajinipriya, M.; Nagalakshmaiah, M.; Robert, M.; Elkoun, S. Importance of Agricultural and Industrial Waste in the Field of Nanocellulose and Recent Industrial Developments of Wood Based Nanocellulose: A Review. *ACS Sustainable Chem. Eng.* **2018**, *6*, 2807–2828. DOI: [10.1021/acssuschemeng.7b03437](https://doi.org/10.1021/acssuschemeng.7b03437).
- [13] Ul-Islam, M.; Ullah, M. W.; Khan, S.; Manan, S.; Khattak, W. A.; Kamal, T.; Wazwaz, A. A.; Abrehem, A. S. Nanocellulose as a Green Material to Eradicate Environment and Renewable Energy Issues. In *Nanocellulose: Synthesis, Structure, Properties and Applications*; Singapore: World Scientific, **2021**; 287–322 DOI: [10.1142/9781786349477_0009](https://doi.org/10.1142/9781786349477_0009).
- [14] Moon, R. J.; Martini, A.; Nairn, J.; Simonsen, J.; Youngblood, J. Cellulose Nanomaterials Review: Structure, Properties and Nanocomposites. *Chem. Soc. Rev.* **2011**, *40*, 3941–3994. DOI: [10.1039/C0CS00108B](https://doi.org/10.1039/C0CS00108B).
- [15] Suter, E. K.; Rutto, H. L.; Seodigeng, T. S.; Kiambi, S. L.; Omwoyo, W. N. Recycled Pulp and Paper Sludge, Potential Source of Cellulose: Feasibility Assessment and Characterization. *J. Environ. Sci. Health. A Tox. Hazard. Subst. Environ. Eng.* **2023**, *58*, 1061–1071. DOI: [10.1080/10934529.2024.2309857](https://doi.org/10.1080/10934529.2024.2309857).
- [16] Dube, A. M.; Daba, B. J.; Muleta, M. D. Optimized Isolation and Characterization of Cellulose for Extraction of Cellulose Nanocrystals from Ensete Ventricosum Pseudo-Stem Fibre Using a Two-Stage Extraction Method. *J. Exp. Nanosci.* **2023**, *18*, 2199989. DOI: [10.1080/17458080.2023.2199989](https://doi.org/10.1080/17458080.2023.2199989).
- [17] Evans, S. K.; Wesley, O. N.; Nathan, O.; Moloto, M. J. Chemically Purified Cellulose and Its Nanocrystals from Sugarcane Bagasse: Isolation and Characterization. *Heliyon* **2019**, *5*, e02635. DOI: [10.1016/j.heliyon.2019.e02635](https://doi.org/10.1016/j.heliyon.2019.e02635).
- [18] Johar, N.; Ahmad, I.; Dufresne, A. Extraction, Preparation and Characterization of Cellulose Fibres and Nanocrystals from Rice Husk. *Ind. Crop. Prod.* **2012**, *37*, 93–99. DOI: [10.1016/j.indcrop.2011.12.016](https://doi.org/10.1016/j.indcrop.2011.12.016).
- [19] Glaus, M. A.; Van Loon, L. R. Cellulose Degradation at Alkaline Conditions: Long-Term Experiments at Elevated Temperatures. **2004**. ISSN 1019-0643
- [20] Jawaid, M.; Khalil, H. A. Cellulosic/Synthetic Fibre Reinforced Polymer Hybrid Composites: A Review. *Carbohydr. Polym.* **2011**, *86*, 1–18. DOI: [10.1016/j.carbpol.2011.04.043](https://doi.org/10.1016/j.carbpol.2011.04.043).
- [21] Dittrich, C.; Pecenka, R.; Selge, B.; Ammon, C.; Kruggel-Emden, H. Influence of Processing Parameters on Fibre Properties during Twin-Screw Extrusion of Poplar Wood Chips. *Horticulturae* **2022**, *8*, 762. DOI: [10.3390/horticulturae8090762](https://doi.org/10.3390/horticulturae8090762).
- [22] Ullah, M. W.; Manan, S.; Ul-Islam, M.; Revin, V. V.; Thomas, S.; Yang, G. Introduction to Nanocellulose. In *Nanocellulose: Synthesis, Structure, Properties and Applications*; Singapore: World Scientific, **2021**; 1–50 DOI: <https://doi.org/10.1142/q0278>.
- [23] Rosli, N. A.; Ahmad, I.; Abdullah, I. Isolation and Characterization of Cellulose Nanocrystals from Agave Angustifolia Fibre. *BioResources* **2013**, *8*, DOI: [10.15376/biores.8.2.1893-1908](https://doi.org/10.15376/biores.8.2.1893-1908).
- [24] Stuart, B. H. *Infrared Spectroscopy: Fundamentals and Applications*. Hoboken: John Wiley & Sons, **2004**; pp. 145–229. ISBN 0-470-85428-6
- [25] Zeng, Y.; Yang, X.; Yu, H.; Zhang, X.; Ma, F. The Delignification Effects of White-Rot Fungal Pretreatment on Thermal Characteristics of Moso Bamboo. *Bioresour. Technol.* **2012**, *114*, 437–442. DOI: [10.1016/j.biortech.2011.10.036](https://doi.org/10.1016/j.biortech.2011.10.036).
- [26] Zainith, S.; Purchase, D.; Saratale, G. D.; Ferreira, L. F. R.; Bilal, M.; Bharagava, R. N. Isolation and Characterization of Lignin-Degrading Bacterium Bacillus Aryabhatai from Pulp and Paper Mill Wastewater and Evaluation of Its Lignin-Degrading Potential. *3 Biotech.* **2019**, *9*, 92. DOI: [10.1007/s13205-019-1631-x](https://doi.org/10.1007/s13205-019-1631-x).
- [27] Jele, T. B.; Sithole, B.; Lekha, P.; Andrew, J. Characterisation of Pulp and Paper Mill Sludge for Beneficiation. *Cellulose* **2022**, *29*, 4629–4643. DOI: [10.1007/s10570-022-04578-7](https://doi.org/10.1007/s10570-022-04578-7).
- [28] Asem, M.; Jimat, D. N.; Jafri, N. H. S.; Nawawi, W. M. F. W.; Azmin, N. F. M.; Abd Wahab, M.; F. Entangled Cellulose Nanofibers Produced from Sugarcane Bagasse via Alkaline Treatment, Mild Acid Hydrolysis Assisted with Ultrasonication. *J. King Saud Univ.-Eng. Sci.* **2021**. DOI: [10.1016/j.jksues.2021.03.003](https://doi.org/10.1016/j.jksues.2021.03.003).
- [29] Phanthong, P.; Reubroycharoen, P.; Hao, X.; Xu, G.; Abudula, A.; Guan, G. Nanocellulose: Extraction and Application. *Carbon Resour. Convers.* **2018**, *1*, 32–43. DOI: [10.1016/j.crcon.2018.05.004](https://doi.org/10.1016/j.crcon.2018.05.004).
- [30] French, A. D. Idealized Powder Diffraction Patterns for Cellulose Polymorphs. *Cellulose* **2014**, *21*, 885–896. DOI: [10.1007/s10570-013-0030-4](https://doi.org/10.1007/s10570-013-0030-4).
- [31] Boudaira, B.; Harabi, A.; Bouzerara, F.; Zenikheri, F.; Foughali, L.; Guechi, A. Preparation and Characterization of Membrane Supports for Microfiltration and Ultrafiltration Using Kaolin (DD2) and CaCO₃. *Desalination Water Treat* **2016**, *57*, 5258–5265. DOI: [10.1080/19443994.2015.1021998](https://doi.org/10.1080/19443994.2015.1021998).
- [32] Bouzerara, F.; Boulanager, S.; Harabi, A. Shaping of Microfiltration (MF) ZrO₂ Membranes Using a Centrifugal Casting Method. *Ceram. Int.* **2015**, *41*, 5159–5163. DOI: [10.1016/j.ceramint.2014.11.141](https://doi.org/10.1016/j.ceramint.2014.11.141).

- [33] Liu, Z.; Hughes, M.; Tong, Y.; Zhou, J.; Kreutter, W.; Lopez, H. C.; Singer, S.; Zitomer, D.; McNamara, P. Paper Mill Sludge Biochar to Enhance Energy Recovery from Pyrolysis: A Comprehensive Evaluation and Comparison. *Energy* **2022**, *239*, 121925. DOI: [10.1016/j.energy.2021.121925](https://doi.org/10.1016/j.energy.2021.121925).
- [34] Li, M.-C.; Wu, Q.; Song, K.; Lee, S.; Qing, Y.; Wu, Y. Cellulose Nanoparticles: Structure–Morphology–Rheology Relationships. *ACS Sustainable Chem. Eng.* **2015**, *3*, 821–832. DOI: [10.1021/acssuschemeng.5b00144](https://doi.org/10.1021/acssuschemeng.5b00144).
- [35] Alemdar, A.; Sain, M. Isolation and Characterization of Nanofibers from Agricultural Residues–Wheat Straw and Soy Hulls. *Bioresour. Technol.* **2008**, *99*, 1664–1671. DOI: [10.1016/j.biortech.2007.04.029](https://doi.org/10.1016/j.biortech.2007.04.029).
- [36] Ngo, T. N. L. T.; Chiang, K.-Y. Co-thermal Degradation Characteristics of Rice Straw and Sewage Sludge. *Sustain. Environ. Res.* **2021**, *31*, 1–14. DOI: [10.1186/s42834-021-00096-6](https://doi.org/10.1186/s42834-021-00096-6).
- [37] Brebu, M.; Vasile, C. Thermal Degradation of Lignin—A Review. *Cellul. Chem. Technol. Romania.* **2010**, *44*, 353.
- [38] Liu, H.; Liu, D.; Yao, F.; Wu, Q. Fabrication and Properties of Transparent Polymethylmethacrylate/Cellulose Nanocrystals Composites. *Bioresour. Technol.* **2010**, *101*, 5685–5692. DOI: [10.1016/j.biortech.2010.02.045](https://doi.org/10.1016/j.biortech.2010.02.045).
- [39] Yaşar, S. Esterification of Cellulose Isolated from Black Poplar (*Populus nigra* L.) Sawdust with Octanoyl Chloride. *Turk. J. For.* **2021**, *22*, 306–310. DOI: [10.18182/tjf.948411](https://doi.org/10.18182/tjf.948411).